Current Science
CS 5 (4), 4169-4182 (2025)
Received 16 May 2025 | **Revised 18 June** 2025 | **Accepted 15 July**. 2025 | **Online Available 28 August** 2025
https://doi.org/ 10.52845/CS/2025-5-4-65

Current Science

Current Science

OPEN ACCESS

ISSN(O)2795-8639

Original Article

Design and Performance Testing of a Drainage Ditching Device for Tobacco-Rice Rotation Fields

Ting Guo[1], Lin Zhu[1], Chao Long[1], Xiangfei Yang[1], Juming Luo[2*]

[1]Hunan Tobacco Company Chenzhou Branch, Chenzhou 423000, China

[2]College of Engineering and Technology, Southwest University, Chongqing 400716, China

[*]Corresponding Author: Juming Luo

Abstract:
To address the issue of high power consumption during ditching operations in tobacco-rice rotation systems in Southern China, a drainage ditching device suitable for these fields was designed and developed based on the soil characteristics and cultivation patterns of the region. The device primarily consists of a traction frame, a cutter disc, ditching blades, a flow-guiding device, and a ditch-clearing plough. The ditching blades are arranged in a spiral pattern with intervals, comprising 7 groups of 2 blades each, totaling 14 blades. Based on the device design and determination of soil parameters, soil particle models and a soil-device interaction model were established using discrete element method (DEM) simulation software. Simulations and analyses were conducted to investigate the effects of forward speed, cutter disc rotational speed, and blade combination on power consumption during the ditching operation. The results indicate that forward speed, blade combination, and cutter disc rotational speed significantly impact power consumption. The optimal parameter combination was determined as follows: forward speed of 0.223 m/s, cutter disc rotational speed of 2.5 r/s, and blade combination type c, resulting in a power consumption of 24 kW for the drainage ditching operation.

Keywords: Ditching equipment; Tobacco-Rice Rotation; Discrete element method; Simulation analysis

1. Introduction

The tobacco-rice rotation system is a commonly adopted cultivation pattern in Southern China. It primarily involves alternating tobacco with late-season rice in a paddy-upland rotation system. This practice enhances resource utilization efficiency, improves soil physicochemical properties, and reduces the incidence of pests and diseases[1,2]. Tobacco plants demand relatively high soil conditions, preferring fertile and well-drained soil. Consequently, ditch excavation for drainage becomes a crucial step in the tobacco-rice rotation process. However, in most tobacco-rice rotation areas, ditching operations still rely heavily on manual labor, suffering from low operational efficiency and high labor intensity. Therefore, research into mechanized ditching technology for tobacco-rice rotation fields is of significant importance.

Commonly used ditching devices fall into three main categories: plow-type, disc-type, and chain-type. Among these, disc-type ditching devices are widely applied in agricultural production due to their advantages of greater trenching depth, higher operational efficiency, and compact structure[3,4,5]. Han et al.[6] optimized the structural parameters of a combined seeding-ditching device based on the Discrete Element Method (DEM), verifying the reliability of the simulation results through experiments, with no blockage observed in the drainage ditches. Shi et al.[7] designed a plow-type ditching device that effectively improved poor ditching performance and high traction resistance

in sweet potato fields. Wang et al.[8] designed a spiral-propeller-like ditching device for furrow opening, which, after optimization, exhibited significantly reduced power consumption, good ditching performance, and stable furrow shape.

Regarding research on ditching mechanisms, the Discrete Element Method (DEM) has become a mainstream approach for analyzing the interaction between ditching devices and soil[9]. Wei et al.[10] established an interaction model between soil and a contour-following ditching device using EDEM-RecurDyn co-simulation and determined the optimal working parameter combination through single-factor quadratic orthogonal rotation combination tests. Barr et al.[11] analyzed the influence of ditching device structural parameters on soil disturbance characteristics based on a DEM-constructed virtual soil bin. Wang et al.[12] established a DEM model for a plow-type ditching device, revealing the influence mechanisms of forward speed, blade opening angle, and width on ditching resistance through single-factor and multi-factor experiments. Ahmad et al.[13] simulated the operational performance of ditching devices with different structures using the Hertz-Mindlin contact model; the results aligned with experimental data, validating the model's reliability.

Building upon previous research and aiming to address the issue of high power consumption during ditching operations in tobacco-rice rotations in Southern China, this study designed a ditching device. The design incorporated the soil characteristics and cultivation patterns specific to these regions and synthesized the structural features of existing straight blades and curved blades. Based on the device design and determination of soil parameters, soil particle models and a soil-device interaction model were established using DEM simulation software. Simulations and analyses were conducted to investigate the effects of forward speed, cutter disc rotational speed, and blade combination type on the power consumption of the ditching operation. The influence of various device parameters on ditching power consumption was studied, and field validation tests were performed to verify the reliability of the simulation results. This study provides a reference for the design of drainage ditching devices in tobacco-rice rotation fields.

2. Materials and Methods

2.1 Structure and Working Principle of the Ditching Device

2.1.1 Ditching Device

The drainage ditching device for tobacco-rice rotation fields (as shown in Figure 1) primarily consists of a cutter disc, ditching blades, a traction frame, a crossbeam, a flow-guiding device, a cutting drive mechanism, longitudinal beams, and a ditch-clearing plough unit. The ditching blades are arranged in a spiral pattern with sequential intervals.

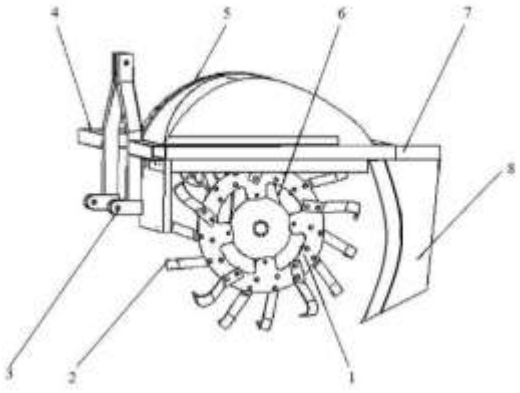

Figure 1. Structure of the drainage ditching device for tobacco-rice rotation fields

1. Cutterhead 2. Ditching knife 3. Traction frame 4. Crossbeam 5. Flow guide device 6. Cutting drive mechanism 7. Longitudinal beam 8. Ditch cleaning plow

Table 1. Main Design and Technical Parameters

Parameter	Value
Overall dimension(L×W×H)/mm	1800×1300×1550
Driving force/kW	≥33.5
Working width/mm	200-250
Working depth/mm	300-400

2.1.2 Working Principle

The device is driven by the tractor's rear power take-off (PTO) shaft. During operation, the tractor is started. The hydraulic operating lever of the tractor is used to lower the cutter disc until its bottom is positioned approximately 100 mm above the ground. The cutting drive mechanism is then engaged to rotate the cutter disc. Once the rotational speed of the cutter disc reaches its rated value, the hydraulic system controls the descent of the ditching device until the desired trenching depth is achieved. At this point, the ditching blades make contact with the soil to commence the ditching operation. Ditching blades *A* and *B* (as shown in Figure 2) sequentially cut the soil and scatter it towards the inner side of the flow-guiding device, which directs the soil towards the inner side of the drainage ditch. Simultaneously, soil flowing back into the drainage ditch undergoes secondary clearing by the ditch-clearing plough unit located at the rear of the frame, thereby completing the ditching operation.

Figure 2. Structure of the cutterhead

2.2 Parameter Design of the Ditching Device

2.2.1 Selection of Blade Diameter

According to the Agricultural Machinery Design Handbook[14], the designed blade diameter D_1 is determined as:

$$D_1 = (1.25\sim1.45)H \quad (1)$$

(1) where H is the ditching depth (m).

Based on the required drainage ditch depth range of 0.55 m to 0.6 m, the cutter disc diameter D_1 was determined as 1.33 × 0.55 = 0.73 m. The cutter disc operating diameter was designed as 1.2 m. To reduce the mass of the cutter disc, it was manufactured as a circular disc with an inner ring diameter D_2 = 0.45 m.

Currently, existing straight-blade and curved-blade structures are primarily suitable for ditching depths less than 0.25 m. For depths exceeding 250 mm, issues such as high energy consumption and unstable trench depth arise, failing to meet the requirements of modern agriculture for energy-saving, drag reduction, and the specific agronomic needs of tobacco field drainage. Based on the existing curved-blade structure, and considering the soil characteristics and cultivation patterns of tobacco-rice rotation fields in Southern China, this study designed the blade thickness, bending angle, and bending radius. Furthermore, a spiral-type discontinuous uniformly arranged blade configuration was designed to reduce the power consumption of the ditching operation and improve ditching quality.

Existing disc-type ditching devices typically employ a uniformly distributed tool mounting method. Building upon this, and based on the soil characteristics of Southern China's tobacco-rice rotation fields and the agronomic requirements for tobacco field drainage, a segmented cutting ditching mechanism was adopted. This mechanism comprises the cutter disc, Ditching Blade *A*, and Ditching Blade *B* (as shown in Figure 2). Ditching Blades *A* and *B* are arranged in a sequential spiral interval pattern (i.e., *A*-*B*-*A*-*B*-..., as shown in Figure 2). During the soil

cutting process, Blade *A* and Blade *B* sequentially cut segments of soil of specific widths. (The sum of the widths cut by the two blade types equals the required working width of the ditch). This segmented cutting approach allows each blade to cut only a portion of the total soil width required for the final ditch. Furthermore, the rational arrangement of the blades ensures that each blade cuts the soil only once.

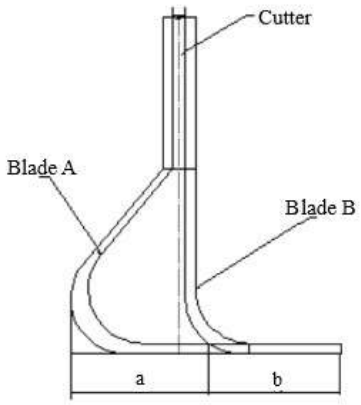

Figure 3. Schematic diagram of ditching tools arranged at the same level

2.2.2 Determination of Structural Parameters for the Spiral-Type Discontinuous Uniform Blade Configuration

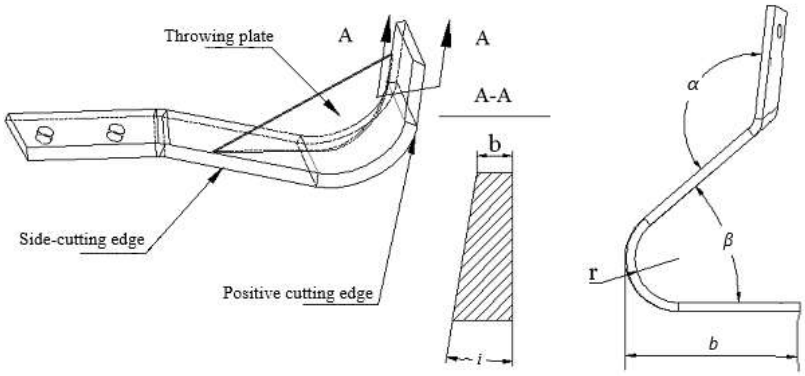

Figure 4. Structural diagram of the ditching tool

The ditching blade primarily consists of a main cutting edge, a side cutting edge, and a soil-throwing plate. Based on the agronomic requirements for tobacco field drainage, the structural parameters of the ditching blade were determined through analysis. These parameters include the rotation radius (*R*), curvature angle (α), main cutting edge angle (*i*), bend radius (*r*), cutting angle (β), and working width (*b*) (as shown in Figure 4). The main structural parameters were finalized, and the blade's structural parameters are listed in Table 2.

(1) Rotation Radius (*R*): Primarily determined based on the ditching depth required for agronomic drainage. With a fixed ditching depth and forward speed, a larger rotation radius should be selected whenever possible. For this design, R = 600 mm was selected.

(2) Curvature Angle (α): Defined as the angle between the cutting surface and the line connecting the blade tip to the axis of the cutter disc. If α is too small, it leads to an excessively large cutting angle for the edge, increasing soil cutting resistance and power consumption. Conversely, if α is too large, the outer grinding edge compacts uncut soil, increasing the pressure exerted on the blade and consequently reducing its service life. Therefore, α should be selected within the range of 40° to 90°.

(3) Main Cutting Edge Angle (*i*): A smaller *i* results in a sharper blade and lower power consumption; however, if it is excessively small, the blade's service life is shortened. Based on the Agricultural Machinery Design Handbook and ditching operation requirements, i = 15° was adopted for this design.

(4) Bend Radius (r): If r is too small, the strength of the ditching blade at the bend is reduced during operation in sticky soils, shortening its service life. However, if r is too large, it increases the unevenness of the ditch bottom and also increases power consumption. A bend radius of r = 50 mm is recommended.
(5) Cutting Angle (β): An increase in β leads to greater ditching resistance and reduced soil fragmentation effectiveness. Conversely, if β is too small, the blade is prone to root entanglement, degrading operation quality. Therefore, β should be selected within the range of 130° to 180°.
(6) Working Width (b): Increasing b can reduce the number of blades required on the cutter disc. However, an excessively large b can compromise the rigidity required for effective soil fragmentation by the blade. Therefore, a working width b in the range of 90 mm to 190 mm is recommended.

Table 2. Structural Parameters of Tools

Tool Combination	a	b	c
Tool *A*'s Cutting Angle β / (°)	130	140	150
Tool *A*'s Bending Angle α / (°)	40	50	60
Tool *A*'s Working Width *b*/(mm)	182	156	133
Tool *B*'s Cutting Angle β/ (°)	180	180	180
Tool *B*'s Bending Angle α / (°)	90	90	90
Tool *B*'s Working Width *b*/(mm)	117.5	143	166

2.3 Soil-Ditching Device Model Construction

2.3.1 Ditching Device Simulation Model

The cutter disc assembly is a critical component of the ditching device, comprising the cutter disc and the ditching blades. To enhance simulation efficiency, components such as the traction frame, flow-guiding device, and cutting drive mechanism were simplified during the simulation process. Connecting parts like bolts, washers, and nuts were omitted. The three-dimensional model of the cutter disc was created using SolidWorks 2020 software, exported in .igs format, and subsequently imported into EDEM 2020 software. The structural parameters were set as follows: cutter disc diameter (D) = 1200 mm, curvature angle (α) = 40°–90°, cutting angle (β) = 130°–180°, bend radius (r) = 50 mm, main cutting edge angle (i) = 15°, and working width (b) = 90–190 mm.

2.3.2 Soil Particle Model

Soil samples were collected from tobacco-rice rotation fields located in Fangyuan Town, Guiyang County, Chenzhou City, Hunan Province (25°39′32″N, 112°39′30″E). The average soil hardness at a depth of 40 cm was measured as 2.448 MPa using an SC900 soil hardness tester. The average soil moisture content was determined to be 17.7% using a TDR300 soil moisture meter. Based on these measurements and referencing the China Soil Database, the soil was identified as yellow earth. The texture of the soil layer from 0 to 50 cm depth is classified as slate shale lateritic red soil, characterized by deep profile, heavy texture, and strong water and nutrient retention capacity. Consequently, four soil particle models were established: single sphere particle, double sphere particle, triangular sphere particle, and horizontally arranged three-sphere clump. To avoid excessive computational demands associated with overly small particle diameters[15], the physical radius of the soil particles was set to 10 mm.

To accurately simulate the mechanical stress of soil particles under mechanical action, the Hysteretic Spring contact model was selected, corresponding to the tested soil type. Particle properties were preset for elastic deformation. When the stress value exceeds a defined threshold, the particle properties transition to plastic deformation. This model allows particles to achieve significant overlap without requiring excessive external force, thereby reflecting the compressibility characteristics of the granular material. The Hysteretic Spring normal force calculation is based on the Walton-Braun theory. The unloading force decreases to zero before the displacement returns to the initial contact point. The exact location of each previous contact point is not "remembered"; consequently, particles behave as new, undeformed spheres after separation. Subsequent contacts will load with a slope K_1, while any reloading before particle

separation will proceed with a slope K_2. Loading continues along this slope K_2 until it reaches the original loading slope K_1, as illustrated in Figure 5.

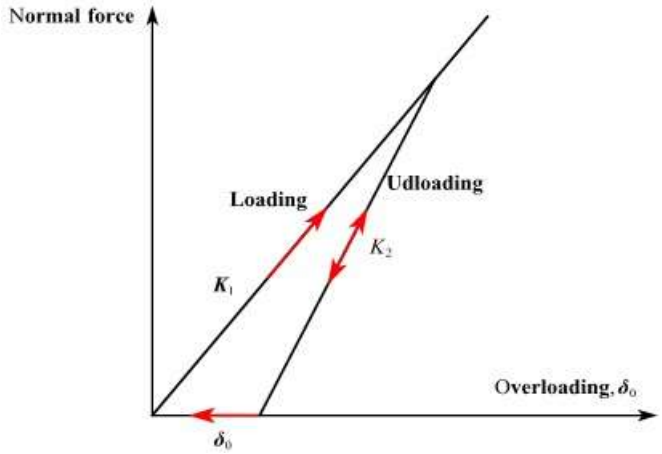

Figure 5. Schematic diagram of force-displacement relationship for the hysteretic spring contact model

The calculation method of the normal force F_N is as follows:

$$F_N = -\begin{cases} K_1\delta_n & (K_1\delta_n < K_2(\delta_n - \delta_0)) \\ K_2(\delta_n - \delta_0) & (\delta_n > \delta_0) \\ 0 & (\delta_n \le \delta_0) \end{cases} \quad (2)$$

$$\delta_0 = \begin{cases} \delta_n(1 - K_1/K_2) & (K_1\delta_n < K_2(\delta_n - \delta_0)) \\ \delta_0 & (\delta_n > \delta_0) \\ \delta_n & (\delta_n > \delta_0) \end{cases} \quad (3)$$

where K_1 and K_2 represent the loading and unloading stiffness, respectively; δn is the normal overlap; and δo is the residual overlap.

2.3.3 Soil-Cutter Disc Simulation Model

When establishing the soil-cutter disc model, the cutting mode of the cutter disc and the requirements for boundary condition handling were considered. The soil simulation model was configured as a skinned rectangular volume measuring 1500 mm (length) × 2000 mm (width) × 600 mm (height). A total of 1.8 × 10^6 soil particles were generated within this volume to simulate the trenching and soil cutting environment. The forward speed and rotational speed of the cutter disc were explicitly defined for the simulation.

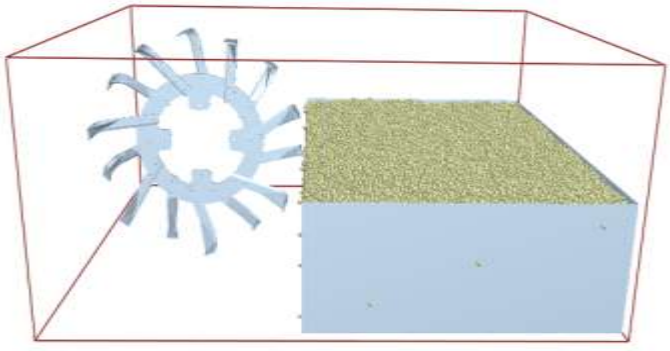

Figure 6. Simulation model of soil-cutterhead interaction

The soil-cutter disc interaction simulation model is illustrated in Figure 6. The EDEM simulation parameters were categorized into material parameters and contact parameters. The material parameters included soil density, cutter disc density, Poisson's ratio, and shear modulus. The contact parameters comprised the coefficients of restitution, static friction, and rolling friction for both soil-soil interactions and soil-cutter disc interactions. The parameters required for the simulation were determined by integrating experimental measurement data with values from the literature[16,17,18].

The simulation time step was set to 1×10^{-6} seconds. The primary parameter values used in the simulation are listed in Table 3.

Table 3. Simulation Parameters

Item	Parameter	Value
Soil particles	Poisson's ratio	0.38
	Shear modulus/ Pa	1×10^{6}
	Density（Kg/m^3）	1850
Cutterhead	Poisson's ratio	0.3
	Shear modulus/ Pa	7.99×10^{10}
	Density（Kg/m^3）	7800
Soil-soil	Restitution coefficient	0.6
	Static friction coefficient	0.6
	Dynamic friction coefficient	0.4
Soil-cutterhead	Restitution coefficient	0.3
	Static friction coefficient	0.5
	Dynamic friction coefficient	0.01

2.4 Ditching Performance Optimization Experiment

2.4.1 Box-Behnken Design (BBD) Experimental Design

Based on the agronomic requirements for tobacco field drainage and the actual production conditions, a Response Surface Methodology (RSM) approach was employed. Three factors were set at three levels each for simulation analysis. The factor-level coding table is presented in Table 4.

Table 4 Simulation Factor Levels

Table 4. Simulation Factor Levels

Level	Factors		
	Forward Speed *v*/（$m\cdot s^{-1}$）	Cutterhead Rotational Speed*n*/（$r\cdot s^{-1}$）	Tool Combination
1	0.22	1.83	a
2	0.32	2.165	b
3	0.42	2.5	c

2.4.2 Evaluation Metrics

To investigate the variation patterns of the ditching device's power consumption under different structural and operational parameters, the experiment selected the following research factors: forward speed, cutter disc rotational speed (operational parameters), and three blade combination types with distinct structural parameters (structural parameter). In accordance with the test metrics stipulated in the Chinese Agricultural Industry Standard Field Ditching Machinery Operational Quality (NY/T 740-2003), the following evaluation metrics were adopted: power consumption, trench width, trench depth, trench depth stability coefficient, and trench width stability coefficient. Trench depth and trench width were calculated according to Equation (4). The trench depth stability coefficient and trench width stability coefficient were calculated

according to Equation (5).

$$h = \frac{\sum_{i=1}^{n} h_i}{N} \quad (4)$$

where h is the average trench depth/width (mm); h_i is the trench depth/width at the i measurement point (mm); and N is the number of measurement points.

$$\begin{cases} S = \sqrt{\frac{\sum_{i=1}^{n}(h_i - h)^2}{N-1}} \\ V = \frac{S}{h} \times 100\% \\ U = 1 - V \end{cases} \quad (5)$$

where S denotes the standard deviation of trench depth/width (mm); V represents the coefficient of variation of trench depth/width (%); U is the stability coefficient (%).

2.4.3 Field Validation Test

The field test was conducted on December 5, 2024, in Fangyuan Town, Guiyang County, Chenzhou City, Hunan Province (25°39′32″N, 112°39′30″E). The soil moisture content of the test field was 15.7%. The main equipment included a TN654 tractor, the ditching device, a tape measure (measuring range: 0-50 m), and an NJTY3 Universal Dynamic Telemetry System (used to measure the power consumption during the ditching operation), as shown in Figure 7. The height of the ditching device center above the ground was set to 200 mm. The operational parameters were set as follows: forward speed of 0.22 m/s, cutter disc rotational speed of 2.5 r/s, and blade combination type c. The test was replicated three times. Along the excavated drainage ditch, 10 equally spaced measurement points were selected, and experimental data were collected at these points.

a **b**

Figure 7. Field validation test. (a) Installation position of the telemetry system; (b) Ditching test

3. Results and Discussion

3.1 Cutting Simulation Process

Within the coordinate system of the cutting simulation model, the working principle of the cutter disc is as follows: The cutter disc advances along the v-direction while rotating counterclockwise to cut the soil, as illustrated in Figure 8(a). As the disc rotates counterclockwise to trench the soil, the main cutting edge of the ditching blade makes initial contact with the soil. Subsequently, the side cutting edge of the blade diagonally compresses the soil above it, continuously fragmenting the soil mass. The cut soil is then propelled by the counterclockwise rotation of the ditching blade and ejected towards both sides via the soil-throwing plate. Ditching Blades A and B, arranged in an alternating spiral pattern, sequentially cut the soil, collectively achieving the required working width for the

trenching operation.

As shown in Figure 8(b), the soil is fully fragmented and exhibits a tendency to move along the ditching blade. This demonstrates the soil-scattering effect exerted by the ditching blades during actual operation. Due to limitations inherent in this experimental study, components impacting simulation efficiency (such as the flow-guiding device) were simplified. Consequently, soil backflow phenomena were more pronounced in the simulation compared to real-world conditions.

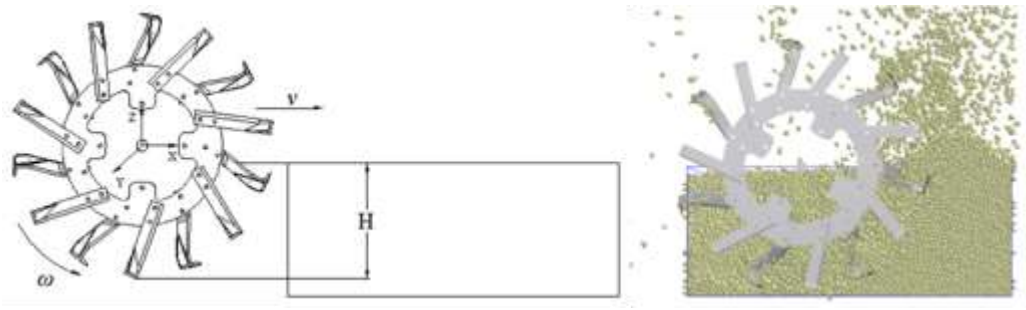

a **b**

Figure 8 Cutting simulation. (a) Schematic diagram of soil cutting;(b) Schematic diagram of cutting and soil throwing

3.2 Simulation Results and Analysis

3.2.1 Regression Analysis

Table 5. Simulation Results

Test No.	Test Factors			Test Index
	Forward Speed X_1/（m·s^{-1}）	Cutterhead Rotational Speed X_2/（r·s^{-1}）	Tool Combination X_3	Operating Power Consumption Y/（kW）
1	0.22	1.83	b	21.18
2	0.32	1.83	b	29.56
3	0.22	2.165	b	33.05
4	0.42	2.5	b	39.4
5	0.22	2.165	c	22.14
6	0.42	2.165	c	38.33
7	0.22	2.165	a	38.91
8	0.42	2.165	a	43.37
9	0.32	1.83	c	26.79
10	0.32	2.5	c	32.44
11	0.32	1.83	a	34.27
12	0.32	2.5	a	33.32
13	0.32	2.165	b	32.74
14	0.32	2.165	b	43.03
15	0.32	2.165	b	33.82
16	0.32	2.165	b	42
17	0.32	2.165	b	39.41

To further determine the effect magnitude of each factor level on power consumption, the experimental data in Table 5 were subjected to fitting analysis and analysis of variance (ANOVA) using Design-Expert software[19,20]. This enabled the derivation of a coded parameter regression equation characterizing the influence of each experimental factor on ditching power consumption:

$$Y = 38.2 + 5.56X_1 + 2.16X_2 - 3.77X_3 - 1.84X_1X_2 + 2.93X_1X_3 + 1.65X_2X_3 - 0.7506X_1^2 - 5.23X_2^2 - 1.47X_3^2 \quad (6)$$

Table 6. Analysis of Variance (ANOVA) for Performance Metrics

Source of Variation	Sum of Squares	Degrees of Freedom	Mean Square	F-Value	P-Value	Significance
Model	592.27	9	65.81	3.76	0.0474	*
X_1	185.77	1	185.77	10.61	0.0139	*
X_2	27.98	1	27.98	1.6	0.2467	—
X_3	113.78	1	113.78	6.5	0.0382	*
X_1X_2	1.15	1	1.15	0.0658	0.8049	—
X_1X_3	34.4	1	34.4	1.96	0.2038	—
X_2X_3	10.89	1	10.89	0.6218	0.4563	—
X_1^2	0.6501	1	0.6501	0.0371	0.8527	—
X_2^2	32.6	1	32.6	1.86	0.2147	—
X_3^2	3.15	1	3.15	0.1796	0.6844	—
Residual	122.6	7	17.51			—
Lack of Fit	34.37	3	11.46	0.5194	0.6913	—
Pure Error	88.23	4	22.06			*
Total	714.87	16				*

Note: Differences were considered highly significant at $P \leq 0.01$ $P \leq 0.01$ (marked with **), significant at $0.01 < P \leq 0.05$ $0.01 < P \leq 0.05$ (marked with *), and non-significant at $P > 0.05$ $P > 0.05$ (marked with -).

From the analysis of variance (ANOVA) presented in Table 6, it can be observed that the model's P-value was significant, while the error term was non-significant. This indicates that each factor significantly affected the power consumption of the ditching operation, and the established model aligns well with actual operational conditions. The model fitting coefficient R = 0.8285 demonstrates good agreement between the regression model and the simulation test results, confirming its suitability for predicting variations in operational power consumption during the ditching process. Table 6 further reveals that: X_1 and X_3 exerted significant effects on ditching power consumption X_2, X_1X_2, X_2X_3, X_1^2, X_2^2, and X_3^2 showed non-significant effects Consequently, based on the ANOVA of factors influencing ditching power consumption, non-significant terms were eliminated from the final model:

$$Y = 38.2 + 5.56X_1 - 3.77X_3 \quad (7)$$

3.2.2 Response Surface Analysis

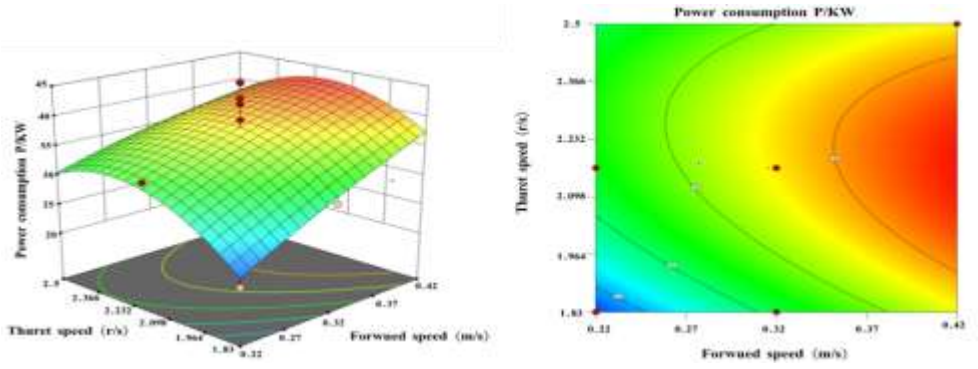

a **b**

Figure 9. Effects of cutterhead rotational speed and forward speed on ditching operation power consumption. (a) Response surface; (b) Contour map

A response surface was constructed based on the regression equation of ditching operation power consumption (as shown in Figure 9). Among all factors, cutterhead rotational speed and forward speed have the most significant impacts on operation power consumption. When the tool combination is type b, the power consumption of ditching operations gradually increases with the increase of cutterhead rotational speed and forward speed. When the cutterhead rotational speed is less than 2.17 r/s, the cutterhead rotational speed has a greater impact on the power consumption of ditching operations. When the cutterhead rotational speed is in the range of $1.83 < X_1 < 2.17$ r/s and the forward speed is in the range of $0.22 < X_2 < 0.319$ m/s, both the cutterhead rotational speed and forward speed have relatively small impacts on the power consumption of ditching operations. Similarly, when the cutterhead rotational speed is greater than 2.17 r/s and the forward speed is greater than 0.319 m/s, their impacts on the power consumption are also small. As shown in the contour map, when the cutterhead rotational speed is in the range of $1.83 < X_1 < 2.5$ r/s and the forward speed is in the range of $0.22 < X_2 < 0.319$ m/s, there is a non-linear relationship between the cutterhead rotational speed and forward speed, and the power consumption of ditching operations is relatively low. When the cutterhead rotational speed is 1.83 r/s and the forward speed is 0.22 m/s, the power consumption of ditching operations reaches the minimum value.

3.3 Parameter Optimization

To identify optimal levels of experimental factors, a parameter optimization study was conducted. A mathematical model for parameter optimization was established, incorporating forward speed (X_2), cutter disc rotational speed (X_1), and blade combination type (X_3). This model, subject to boundary conditions of experimental factors, was analytically solved through regression analysis as follows:

$$\max \mathrm{Y} \begin{cases} 0.22 \le X_1 \le 0.267 \\ 1.83 \le X_2 \le 2.5 \\ 13 \le Y(X_1, X_2) \le 35 \end{cases} \tag{8}$$

In agricultural machinery operations, to achieve the goals of low energy consumption and high operational efficiency, the optimization function provided by Design-Expert software was employed to obtain the optimal combination of influencing factors: a forward speed of 0.223 m/s, a cutterhead rotational speed of 2.5 r/s, a tool combination of type c, and a power consumption of 24 kW for ditching operations. The target requirement is to maximize the depth index of the ditching device during operation while minimizing the power consumption of ditching operations as much as possible.

3.4 Results of Field Validation Tests

The results of the field tests are presented in Table 7 (Figure 10). The operational power consumption of the ditching device ranged from 22.89 to 23.51 kW, with a relative error between the test results and simulation results not exceeding 5%. The ditching depth in the tests was 368.5–375.7 mm, with a relative error within 10% compared to the simulation results; the stability coefficient of ditching depth was 94.6%–95.2%, with a relative error within 3% relative to the simulation results. The ditching width in the tests was 230.9–240.9 mm, with a relative error within 10% compared to the simulation results; the stability coefficient of ditching width was 95.2%–97.3%, with a relative error within 3% relative to the simulation results.

In summary, the field test results are consistent with the simulation results. The ditching depth and width meet the operational requirements, with both the stability coefficients of depth and width not less than 90%. The operational power consumption is close to the optimized power consumption, with a relative error not exceeding 5%, thus satisfying the requirements for tobacco field ditching and drainage.

Figure 10. Test drainage ditch

Table 7. Test Results

No.	Category	Operational Power Consumption /(kW)	Ditching Depth /(mm)	Stability Coefficient of Ditching Depth	Ditching Width /(mm)	Stability Coefficient of Ditching Width
1	Simulation	24.12	371.4	95.4%	242.7	94.9%
	Test	23.51	375.7	94.6%	240.9	95.2%
2	Simulation	23.46	368.8	96.7%	233.4	96.1%
	Test	22.89	371.2	95.2%	231.3	96.5%
3	Simulation	23.62	363.7	96.5%	243.7	96.6%
	Test	23.24	368.5	94.9%	230.9	97.3%

4. Conclusions

(1) Based on the soil characteristics and planting patterns of tobacco-rice rotation fields in southern China, a drainage ditching device for tobacco-rice rotation fields was designed. This device can effectively complete the ditching operation during the tobacco-rice rotation process and realize the mechanization of drainage ditching operations in tobacco-rice rotation fields in southern China.

(2) A discrete element simulation software was used to establish a soil-ditching device interaction model. Through simulation analysis, a mathematical model between ditching operation power consumption and test factors was established, and the influence laws of forward speed, cutterhead rotational speed, and tool combination on ditching operation power consumption were analyzed.

(3) Through the optimization of simulation tests, the optimal parameter combination was obtained: a forward speed of 0.223 m/s, a cutterhead rotational speed of 2.5 r/s, a tool combination of type c, and a ditching operation power consumption of 24 kW.

(4) Field tests showed that the operational power consumption of the ditching device was 22.89–23.51 kW, with a relative error not exceeding 5% compared to the simulation results. The ditching depth and width were 368.5–375.7 mm and 230.9–240.9 mm, respectively, and the stability coefficients of ditching depth and width were not less than 90%, which meet the requirements for tobacco drainage ditching.

Author Contributions: Conceptualization, Ting Guo and Lin Zhu; methodology, Lin Zhu; software, Chao Long; validation, Chao Long; formal analysis, Xiangfei Yang; investigation, Xiangfei Yang; resources, Chao Long; data curation, Ting Guo; writing— original draft preparation, Ting Guo; writing— review and editing, Ting Guo; visualization, Juming Luo; supervision, Juming Luo; project administration, Lin Zhu; funding acquisition, Lin Zhu; All authors have read and agreed to the published version of the manuscript.

Funding: This study was supported by the projects of Hunan Provincial Tobacco Company Chenzhou City Company: development of light and simple tobacco cultivator based on the hilly area of Nanling Mountain (CZYC2022JS05) and

research and application of tobacco fertilization machine and supporting fertilization technology (CZYC2023JS03).

Institutional Review Board Statement: Not applicable.

Informed Consent Statement: Not applicable.

Data Availability Statement: The original contributions presented in the study are included in the article, further inquiries can be directed to the corresponding author.

Conflicts of Interest: The authors declare that they have no known competing financial interests or personal relationships that could have appeared to influence the work reported in this paper.

References

1. Xie, S. Y., Guo, N. J., Liu, H. B., 2016. Potential Distribution Prediction of Medium Aroma Type of Flue-cured Tobacco Based on Ecological Niche Model. Adv. J. Food Sci. Technol., 10(12), 927-933. https://doi.org/10.19026/ajfst.10.2289
2. Zou, C. M., Li, Y., Huang, W., Zhao, G. K., Pu, G. R., Su, J. E., Coyne, M. S., Chen, Y., Wang, L. C., Hu, X. D., Jin, Y., 2018. Rotation and manure amendment increase soil macro-aggregates and associated carbon and nitrogen stocks in flue-cured tobacco production. Geoderma, 325(1), 49-58. https://doi.org/10.1016/j.geoderma.2018.03.017
3. Zhao, J. L., Lu, Y., Guo, M. Z., Fu, J., Wang, Y. J., 2021. Design and experiment of bionic stubble breaking-deep loosening combined tillage machine. Int J Agric & Biol Eng, 14(4), 123-134. https://doi.org/10.25165/j.ijabe.20211404.6473
4. Liu, D. W., Xie, F. P., Ye, Q., Ren, S. G., Li, X., Liu, M. Z., 2019. Analysis and experiment on influencing factors on power of ditching parts for 1K-50 orchard ditching. Transactions of the Chinese Society of Agricultural Engineering, 35(18), 19-28. https://doi.org/10.11975/j.issn.1002-6819.2019.18.003
5. Jia, H. L., Meng, F. H., Liu, L. J., Shi, S., Zhao, J. L., Zhuang, J., 2020. Biomimetic Design and Experiment of Core-share Furrow Opener. Transactions of the Chinese Society for Agricultural Machinery, 51(4), 44-49, 77. https://doi.org/ 10.6041/j.issn.1000-1298.2020.04.005
6. Han, L. J., Yuan, W., Yu, J. J., Jin, J. J., Xie, D. S., Xi, X. B., Zhang, Y. F., Zhang, R. H., 2022. Simulation and Experiment of Spiral Soil Separation Mechanism of Compound Planter Based on Discrete Element Method (DEM). Agriculture, 12(4), 511. https://doi.org/10.3390/agriculture12040511
7. Shi, Y. L., Chen, X. Y., Chen, M. D., Wang, D. W., Shang, S. Q., 2022. Design and Experiment on Ploughshare Furrowing Ridging Device of Sweet Potato Ridging Shaping Machine. Transactions of the Chinese Society for Agricultural Machinery, 53(10), 16-25. https://doi.org/10.6041/j.issn.1000-1298.2022.10.002
8. Wang, L. Z., Liao, Q. X., Zhang, Z. L., Li, M. L., Zhang, Q. S., Wang, L., Liao, Y. T., 2024.Optimization and experiments of the blade group of ditching devices in rapeseed direct seeder. Transactions of the Chinese Society of Agricultural Engineering, 40(3), 37-49. https://doi.org/10.11975/j.issn.1002-6819.202308057
9. Zhao, Z. H., Wu, M. L., Jiang, X. H., 2024. A Review of Contact Models' Properties for Discrete Element Simulation in Agricultural Engineering. Agriculture, 14(2), 238. https://doi.org/10.3390/agriculture14020238
10. Wei, S., Zhang, C. H., Zhan, Z. Y., Nong, F., Ding, Y.C., 2025. Simulation and optimization test of imitation furrowing process of cotton direct seeding machine based on DEM-MBD couping. Transactions of the Chinese Society for Agricultural Machinery, 56(2), 275-289, 341. https://doi.org/10.6041/j.issn.1000-1298.2025.02.026
11. Barr, J., Desbiolles, J., Ucgul, M., Fielke, J. M., 2020. Bentleg furrow opener performance analysis using the discrete element method. Biosystems engineering, 189,99-115. https://doi.org/10.1016/j.biosystemseng.2019.11.008
12. Wang, L. J., Zhou, B., Wan, C., Zhou, L., 2024. Structural parameter optimization of a furrow opener based on EDEM software. Int J Agric & Biol Eng, 17(3), 115-120. https://doi.org/10.25165/j.ijabe.20241703.7927
13. Ahmad, F., Qiu, B. J., Ding, Q. S., Ding W. M., Khan, Z. M., Shoaib, M., Chandio, F. A., Rehim, A., Khaliq, A., 2020. Discrete element method simulation of disc type furrow openers in paddy soil. Int J Agric &

Biol Eng, 13(4), 103-110. https://doi.org/10.25165/j.ijabe.20201304.4800
14. China Academy of Agricultural Mechanization, 2007. Agricultural machinery design manual. China Agricultural Science and Technology Press, pp. 322-335.
15. Ucgul, M., Fielke, J. M., Saunders, C., 2015. Three-dimensional discrete element modelling (DEM) of tillage: Accounting for soil cohesion and adhesion. Biosystems Engineering, 129, 298-306. http://dx.doi.org/10.1016/j.biosystemseng.2014.11.006
16. Fang, H. M., Ji, C. Y., Chandio, F. A., Guo, J., Zhang, Q. Y., Chaudhry, A., 2016. Analysis of soil movement behavior in rotary tillage process based on discrete element method. Transactions of the Chinese Society for Agricultural Machinery, 47(3), 22-28. https://doi.org/10.6041/j.issn.1000-1298.2016.03.004
17. Fielke, J. M., 1996. Interactions of the Cutting Edge of Tillage Implements with Soil. J. agric. Engng Res., 63(1), 61-72. https://doi.org/10.1006/jaer.1996.0008
18. Tama´s, K., Jo´ri, I. J., Mouazen, A. M., 2013. Modelling soil–sweep interaction with discrete element method. Soil & Tillage Research, 134, 223-231. http://dx.doi.org/10.1016/j.still.2013.09.001
19. Li, Y. Y., 2008. Test design and data processing. Chemical Industry Press, pp. 54-57.
20. Ren, L. Q., 2009. Test design and optimization. Science Press, pp. 34-54.